

Fermionic-Adapted Shadow Tomography for dynamical correlation functions

Taehee Ko,^{1,*} Mancheon Han,¹ and Sangkook Choi^{1,†}

¹*School of Computational Sciences, Korea Institute for Advanced Study*

Dynamical correlation functions are essential for characterizing the response of the quantum many-body systems to the external perturbation. As their calculation is classically intractable in general, quantum algorithms are promising in this aspect, but most rely on brute force measurement strategies that evaluate one body observable pair per circuit. In this work, we introduce Fermionic-Adapted Shadow Tomography (FAST) protocols, a new framework for the efficient calculation of multiple dynamical correlation functions. The key idea is to reformulate these functions into forms that are compatible with shadow tomography techniques. The circuits in our protocols require at most two-copy measurements with uncontrolled Hamiltonian simulation. We show that the proposed protocols enhance sample efficiency and reduce the number of measurement circuits by an order of one or two with respect to the number of qubits across a range of scenarios.

I. INTRODUCTION

The simulation of quantum many-body systems is considered as one of the most promising areas for realizing quantum advantage [3, 4, 31, 45]. Among various applications, of critical interest in computational physics is the estimation of dynamical correlation functions. Since they formulate physical properties for measured outcomes from experiments [47], developing efficient simulation tools for the correlation functions is of practical importance for understanding the physics behind systems in experiments. Besides, correlation functions are the building-block for the functional approaches to the quantum many-body theory [8, 46, 52].

For the task, numerous quantum algorithms have been proposed recently. Roughly, the algorithms are classified into variational and sampling-based approaches. Variational approaches optimize parameterized circuits to approximate the correlation functions, which is suitable for near-term quantum computers [13, 22, 26, 39, 49]. However, these approaches lack rigorous guarantees due to their reliance on the choice of ansatz and non-convex optimization procedures. In contrast, sampling-based approaches enable the estimation of correlation functions using guaranteed numerical techniques. These include the Hadamard test combined with the Hamiltonian simulation [5, 14, 28, 42, 43] or the block encoding [55]. In general, these algorithms estimate a correlation function at a given time or frequency point.

Notably, measurements with sophisticated circuit constructions or techniques can facilitate the computation of correlation functions. For example, computing the functions at multiple time points is performed with a single circuit [33, 51, 57], and the methods in [35, 41] apply shadow tomography techniques for computing multiple correlation functions at a time point. A key insight from these approaches is that building clever measurement strategies can lead to efficient and novel algorithms, an idea already explored in a variety of applications such as efficient measurement schemes for variational quantum algorithms [10, 12, 25, 27, 36, 60, 61], measurement-based quantum computing

* kthmomo@kias.re.kr

† sangkookchoi@kias.re.kr

algorithms [6, 16, 21, 24, 40], and shadow tomography techniques for learning tasks [9, 15, 30, 31, 41, 59]. More closely related to this work, the aforementioned methods [35, 41] show some novel aspects compared to the brute-force measurement strategy of estimating correlation functions, but their sample complexity remains polynomially-efficient only for certain cases.

In this work, we introduce a new framework for efficiently estimating the dynamical correlation functions via shadow tomography techniques. We first reformulate the correlation functions into direct measurement forms that enable to incorporate shadow tomography techniques. We highlight that the reformulations allow more efficient protocols than the brute force strategy of measuring one-body observable pairs individually. We refer to our protocols as the Fermionic-Adapted Shadow Tomography (FAST). The FAST is classified into the commutator and anti-commutator cases. For the commutator correlation functions, the FAST achieves at least order one of reduction with respect to the number of fermionic modes n in terms of sample complexity and the number of circuits to execute. In the anti-commutator case, in the regime where $n \geq \frac{1}{\epsilon^2}$ for a given precision ϵ , the FAST achieves an order of one improvement in terms of sample complexity and the number of circuits to execute. When $n \leq \frac{1}{\epsilon^2}$, we found that there is no sample efficiency but the number of circuits can be reduced by an order of one under a proper fermion-to-qubit mapping.

Throughout this work, we do not consider various noises in quantum hardware, which is beyond the scope of this work. Accordingly, we make the following assumption:

Assumption 1. *The circuits in Fig. 1 are implemented on a fault-tolerant quantum computer. Additionally, a problem-dependent state ρ is provided, along with uncontrolled Hamiltonian simulation.*

The main operations in the circuits Fig. 1 involve the preparation of a problem-dependent quantum state [18, 20, 23, 44, 50, 54, 58] (e.g. the ground state of system), the compilation of uncontrolled Hamiltonian simulations [17, 20, 34, 38, 53, 62], and the dynamical circuit strategy in [40]. The first two operations are among the most actively studied areas in quantum computing. The dynamical circuit strategy in [40] allows a single circuit to conduct the random Pauli measurement [31]. Recent advances in quantum hardware are making the implementation of dynamic circuits progressively more practical [2, 7, 19].

Under the assumption, we address the following question:

Question 1. *Can we develop efficient protocols for estimating the dynamical correlation functions than the brute force strategy of measuring one-body observable pair at a time in terms of sample complexity and the number of measurement circuits?*

In terms of sample complexity and circuit complexity, we answer this question by proposing protocols tailored to each of the representative fermion-to-qubit mappings: Jordan-Wigner (JW) , Bravyi-Kitaev (BK) [11], and ternary tree (TT) [37].

II. RESULTS

A. Reformulations of correlation functions

Under a fermion-to-qubit mapping, we consider the dynamical correlation functions,

$$C(A, B, t) = \text{tr}(\rho[A(t), B]) \text{ or } \text{tr}(\rho\{A(t), B\}), \quad (1)$$

where A and B are Pauli observables. The standard form of a correlation function, where A, B are 1-body observables as in the following examples, is reconstructed from a linear combination of

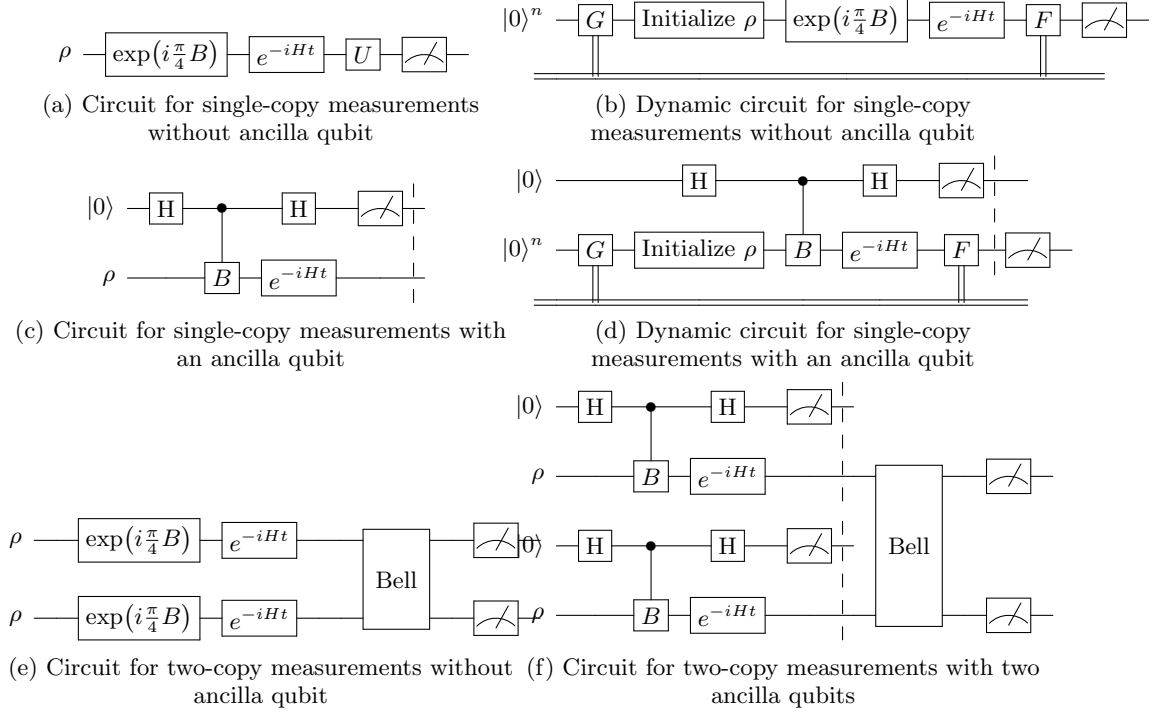


FIG. 1: Circuits for single-copy and two-copy measurements used in our protocols for estimating the dynamical correlation functions. The gate B denotes a given Pauli string. In Fig. 1a, a set of Clifford unitaries for mutually commuting observables, denoted as U , is used. In Fig. 1b, Fig. 1d,

we use the dynamic circuit technique for random Pauli measurement [40]. Following the same notation in [40], we denote by G, F , the operations for generating the probability distribution for which Pauli basis is sampled, and receiving the feedback for constructing the corresponding Pauli basis. In Fig. 1e, we perform the Bell sampling to throw out observables of negligible expectation magnitudes [32, 41]. In Fig. 1f, we also apply Bell sampling in a certain case, while in the other, we use a variant that requires measurement in a problem-dependent basis, as will be shown in

Lemma 5.

$\mathcal{O}(1)$ -many functions in (1). These correlation functions are applied for characterizing dynamical properties of quantum systems.

Example 1 (Density-Density Response). Let $n_i = c_i^\dagger c_i$, $n_j = c_j^\dagger c_j$ be the number operators. The density-density correlation function is:

$$\chi_{ij}(t) = -i \theta(t) \text{tr}(\rho[n_i(t), n_j(0)]), \quad (2)$$

which measures how a density perturbation at site j affects the density at site i at a later time.

Example 2 (Current-Current Correlation). Let $A = J_i = it(c_i^\dagger c_{i+1} - c_{i+1}^\dagger c_i)$ denote the current operator between sites i and $i+1$. Similarly, we denote $B = J_j = it(c_j^\dagger c_{j+1} - c_{j+1}^\dagger c_j)$. The

current-current response function is:

$$\chi_{ij}^R(t) = -i\theta(t) \text{tr}(\rho[J_i(t), J_j(0)]), \quad (3)$$

In a 2D lattice, let $J_{ij} = it_{ij}(c_i^\dagger c_j - c_j^\dagger c_i)$ be the current operator from site i to j with hopping amplitude between sites i and j . The retarded current-current correlation function is then expressed as:

$$\chi_{(i,j)(k,l)}^R(t) = -i\theta(t) \text{tr}(\rho[J_{ij}(t), J_{kl}(0)]), \quad (4)$$

where $J_{ij}(t) = e^{iHt} J_{ij} e^{-iHt}$. This retarded current-current correlation function enters the Kubo formula for the optical conductivity.

Example 3 (Green's functions). The retarded Green's function is defined as

$$G_{ij}^R(t) = -i\theta(t) \text{tr}(\rho\{c_i(t), c_j^\dagger(0)\}), \quad (5)$$

where $c_i(t) = e^{iHt} c_i e^{-iHt}$ is the fermionic annihilation operator in the Heisenberg picture. This function is central to computing spectral functions and local density of states via the Fourier transform. The particle-hole correlation function is given by

$$C_{ij}(t) = \text{tr}(\rho c_i(t) c_j^\dagger(0)), \quad (6)$$

which describes the propagation of a particle excitation from site j to site i .

In this section, we present reformulations of the correlation functions in (1) that are amenable to direct measurement on a quantum computer, and therefore compatible with shadow tomography techniques.

In the commutator case, we reformulate the representation of the correlation functions as,

$$\begin{aligned} C(A, B, t) &= \text{tr}(\rho[A(t), B]) \\ &= -i \left[4 \text{tr} \left(\left(\frac{I + iB^\dagger}{2} \right) \rho \left(\frac{I - iB}{2} \right) A(t) \right) - \text{tr}(\rho A(t)) - \text{tr}(B^\dagger \rho B A(t)) \right]. \end{aligned} \quad (7)$$

Notice that if B is a Pauli string, the formulation simplifies to

$$C(A, B, t) = -i [2 \text{tr}(e^{-iHt} e^{i\frac{\pi}{4}B} \rho e^{-i\frac{\pi}{4}B} e^{iHt} A) - \text{tr}(e^{-iHt} \rho e^{iHt} A) - \text{tr}(e^{-iHt} B \rho B e^{iHt} A)] \quad (8)$$

Therefore, this representation allows us to estimate the commutator correlation function with three types of direct measurements and three circuits: 1. measure observable A with state $e^{-iHt} e^{i\frac{\pi}{4}B} \rho e^{-i\frac{\pi}{4}B} e^{iHt}$, 2. measure observable A with state $e^{-iHt} \rho e^{iHt}$, and 3. measure observable A with state $e^{-iHt} B \rho B e^{iHt}$.

However, the anti-commutator case is not straightforward as the commutator case. To do similarly, we require the operation $\frac{I+B}{2}$ or $\frac{I-B}{2}$ as shown below but these are non-unitary operations that are not directly implementable on quantum computers. In this case, we therefore exploit the notion of measurement-based quantum computing (MBQC) strategy, which leads to two representations of the anti-commutator correlation function. By a bit of algebra, we achieve that

$$\begin{aligned} C(A, B, t) &= \text{tr}(\rho\{A(t), B\}) \\ &= 4 \text{tr} \left(\left(\frac{I + B}{2} \right) \rho \left(\frac{I - B}{2} \right) A(t) \right) - \text{tr}(\rho A(t)) - \text{tr}(B \rho B A(t)), \end{aligned} \quad (9)$$

and

$$\begin{aligned} C(A, B, t) &= \text{tr}(\rho\{A(t), B\}) \\ &= -4 \text{tr}\left(\left(\frac{I-B}{2}\right) \rho\left(\frac{I-B}{2}\right) A(t)\right) + \text{tr}(\rho A(t)) + \text{tr}(B\rho B A(t)) \end{aligned} \quad (10)$$

As we did above, assume that B is a Pauli string. To exploit MBQC, we reformulate these representations as follows,

$$\begin{aligned} C(A, B, t) &= 4C_+^2 \text{tr}(\rho_+ A) - \text{tr}(e^{-iHt} \rho e^{iHt} A) - \text{tr}(e^{-iHt} B \rho B e^{iHt} A) \\ C_+^2 &= \text{tr}\left(\left(\frac{I+B}{2}\right) \rho\left(\frac{I+B}{2}\right)\right), \quad \rho_+ = \frac{e^{-iHt} \left(\frac{I+B}{2}\right) \rho \left(\frac{I+B}{2}\right) e^{iHt}}{C_+}, \end{aligned} \quad (11)$$

and

$$\begin{aligned} C(A, B, t) &= -4C_-^2 \text{tr}(\rho_- A) + \text{tr}(e^{-iHt} \rho e^{iHt} A) + \text{tr}(e^{-iHt} B \rho B e^{iHt} A) \\ C_-^2 &= \text{tr}\left(\left(\frac{I-B}{2}\right) \rho\left(\frac{I-B}{2}\right)\right), \quad \rho_- = \frac{e^{-iHt} \left(\frac{I-B}{2}\right) \rho \left(\frac{I-B}{2}\right) e^{iHt}}{C_-}. \end{aligned} \quad (12)$$

Observe that $C_+^2 + C_-^2 = 1$. These quantities are exactly the probabilities of the output state to be ρ_\pm , which are obtainable from the circuits in Fig. 1c, Fig. 1d, and Fig. 1f. Technically, we check this in Appendix B.

We notice that the output states ρ_\pm from Fig. 1c, Fig. 1d, or Fig. 1f are prepared probabilistically. This implies that we cannot deterministically use the representations in (11) and (12) as the commutator case. Instead, we suggest to follow a majority rule for selecting one of the representations based on resulting statistics. Simply, for a scheduled number of circuit samplings, we count the outcomes in the ancilla. If the state $|0\rangle$ is observed more frequently than $|1\rangle$, we know that $C_+^2 \geq C_-^2$ with high probability and choose the *plus* representation (11). In the opposite case, we choose the *minus* representation (12). More importantly, we can make use of the output states at least half of the scheduled number of samplings. We state this formally in the following lemma.

Lemma 1. *Given scheduled $N_s = \mathcal{O}(\frac{\log \frac{1}{\epsilon}}{\epsilon^2})$ circuit samplings, let n_+ and n_- be the number of outcomes being $|0\rangle$ and $|1\rangle$ in the ancilla qubit, respectively. Then, the following holds with probability at least $1 - \delta$,*

$$\left|C_+^2 - \frac{n_+}{N_s}\right|, \left|C_-^2 - \frac{n_-}{N_s}\right| \leq \epsilon, \quad (13)$$

and either ρ_+ or ρ_- is prepared with at least $\frac{N_s}{2}$ times. Consequently, in either of the fermionic correlation functions in (11) and (12), the first term can be estimated with at least $\frac{N_s}{2}$ samples.

Proof. The first statement immediately follows from the Hoeffding's inequality by considering the random variable X that counts the number of outcomes to be $|0\rangle$. The second statement is true since $\frac{n_+}{N_s} + \frac{n_-}{N_s} = 1$ and either of n_+ or n_- must be $\geq \frac{N_s}{2}$, which means that one of the states ρ_\pm is more often returned with at least $\frac{N_s}{2}$ samples. \square

We remark that from the commutator representation (8), and the anti-commutator ones in (11) and (12), we can straightforwardly estimate the general form of the correlation functions (1) by summing them up,

$$\text{tr}(\rho A(t) B). \quad (14)$$

In particular, if the sample complexities for estimating the commutator and anti-commutator correlation functions are comparable, then the sample complexity for estimating the general correlation functions of the form (14) is of the same scaling.

B. Protocol for the commutator case

We consider the commutator case where correlation functions involve 1-body observables with $i, j, k, l \in [n]$,

$$\text{tr}\left(\rho[e^{iHt}c_i^\dagger c_j e^{-iHt}, c_k^\dagger c_l]\right), \quad (15)$$

where c_i^\dagger and c_j denote the fermionic creation and annihilation operators. In this section, we present a protocol that allows to efficiently estimate these correlation functions. Our protocol exploits existing techniques of learning 1-body observables. The key idea is to incorporate these techniques into the representation (8) and design estimating protocols for the dynamical correlation functions (15).

For a given precision ϵ , we distinguish between two regimes: $n \leq \frac{1}{\epsilon^2}$ and $n \geq \frac{1}{\epsilon^2}$. This is attributed to the recent result by King *et al* [41], which shows that in the latter regime, protocols employing two-copy measurements can outperform those based solely on single-copy measurements.

We first consider the case when $n \leq \frac{1}{\epsilon^2}$. In the following lemma, we restate a result from [10].

Lemma 2. [10, Appendix C] *Assume $n \leq \frac{1}{\epsilon^2}$. Then, there exists a shadow tomography protocol that is compatible with the Jordan-Wigner (JW) mapping and the Bravyi-Kitaev (BK) mapping, and uses single-copy measurements to estimate the 1-body fermionic observables to additive error ϵ with sample complexity,*

$$\mathcal{O}\left(\frac{n \log n}{\epsilon^2}\right), \quad (16)$$

and $\mathcal{O}(n)$ measurement circuits of $\mathcal{O}(n)$ depth.

Proof. From the result in [10, Appendix C], we can construct $\mathcal{O}(n)$ clifford measurement circuits for the 2-Majorana operators, and thus 1-body observables. \square

Another efficient fermion-to-qubit mapping is the ternary tree mapping [37]. Compared to the BK mapping that achieves $\log_2 n + 1$ locality [29] as the worst-case, the ternary tree mapping improves the base factor as $\log_3(2n)$ locality. In turn, this enables estimating the 1-body observables with comparable sample complexity to the protocol in Lemma 2 by incorporating it into the random Pauli measurement in [31]. We can further make it practical for real quantum device by introducing the notion of dynamic circuits [40], which allows to do the task with a single circuit in principle. We summarize this protocol in the following lemma.

Lemma 3. *Assume that $n \leq \frac{1}{\epsilon^2}$. Then, there exists a shadow tomography protocol that is compatible with the ternary tree (TT) mapping, and uses single-copy measurements to estimate the 1-body observables to additive error ϵ with sample complexity,*

$$\mathcal{O}\left(\frac{n \log n}{\epsilon^2}\right), \quad (17)$$

and a single measurement circuit of $\mathcal{O}(1)$ depth.

Proof. Since the TT mapping yields $\log_3(2n)$ -local Paulis, and the sample complexity of the random Pauli measurement [31] scales as $\mathcal{O}(\frac{3^w \log m}{\epsilon^2})$ where w is the locality of Paulis and m is the number of observables, the sample complexity of estimating the 1-body observables is $\mathcal{O}(\frac{n \log n}{\epsilon^2})$. Furthermore, the dynamic circuit [40] allows to perform the random Pauli measurements. \square

For the case where $n \geq \frac{1}{\epsilon^2}$, we restate the results from [41] in the form of the following lemma.

Lemma 4. [41, from Lemmas 1 and 12] *Assume that $n \geq \frac{1}{\epsilon^2}$. Then, there exists a shadow tomography protocol that is compatible with the JW, BK, and TT mappings, uses $\mathcal{O}(\frac{1}{\epsilon^2})$ circuits, single-copy and two-copy measurements to estimate the 1-body observables to additive error ϵ with sample complexity,*

$$\mathcal{O}\left(\frac{\log n}{\epsilon^4}\right), \quad (18)$$

and the depth of each circuit scales as $\mathcal{O}(n)$ at most.

For concreteness, the proof of this lemma is shown in Appendix A, which immediately follows from the original work [41].

By applying these results, we obtain a shadow tomography protocol for estimating the correlation functions in (15) as follows,

Theorem 1. *For a given precision $\epsilon > 0$, there exists a shadow tomography protocol that is compatible with the JW, BK, and TT mappings, uses at most two-copy measurements, and estimates the correlation functions in (15) to the precision ϵ with sample complexity $\mathcal{O}(\frac{n^3 \log n}{\epsilon^2})$ when $n \leq \frac{1}{\epsilon^2}$, and $\mathcal{O}(\frac{n^2 \log n}{\epsilon^4})$ when $n \geq \frac{1}{\epsilon^2}$.*

Proof. In the representation (8), we let $A = c_i^\dagger c_j$ and $B = c_k^\dagger c_l$, and consider the following three terms

$$\begin{aligned} \text{tr}(\rho_1 A), \quad \rho_1 &= e^{-iHt} e^{i\frac{\pi}{4}B} \rho e^{-i\frac{\pi}{4}B} e^{iHt} \\ \text{tr}(\rho_2 A), \quad \rho_2 &= e^{-iHt} \rho e^{iHt} \\ \text{tr}(\rho_3 A), \quad \rho_3 &= e^{-iHt} B \rho B e^{iHt}. \end{aligned} \quad (19)$$

By fixing B , we apply the results in Lemma 2 (JW,BK), Lemma 3 (TT), and Lemma 4 (JW,BK,TT) to estimate the 1-body observables, A 's, three times respectively for the three quantum states ρ_i ($i = 1, 2, 3$). That is, when $n \leq \frac{1}{\epsilon^2}$, $\mathcal{O}(\frac{n \log n}{\epsilon^2})$ samples suffice, and $\mathcal{O}(\frac{\log n}{\epsilon^4})$ in the other scenario. Since there are $\mathcal{O}(n^2)$ choices for B , the total sample complexity for estimating the correlation function (15) scales as $\mathcal{O}(\frac{n^3 \log n}{\epsilon^2})$ when $n \leq \frac{1}{\epsilon^2}$ and $\mathcal{O}(\frac{n^2 \log n}{\epsilon^4})$ when $n \geq \frac{1}{\epsilon^2}$, respectively. \square

C. Protocol for the anti-commutator case

We turn to the anti-commutator case. In this case, the important correlation function is the retarded Green's function (RGF),

$$G_{ab}^R(t) := -i\Theta(t) \text{tr}\left(\rho\{c_i(t), c_j^\dagger\}\right), \quad (20)$$

Protocol 1: Fermionic-adapted shadow tomography 1 (FAST 1)

Data: Given initial state ρ , precision $\epsilon > 0$

Result: approximate the correlation functions (15) for any i, j, k, l

If $n \leq \frac{1}{\epsilon^2}$: **for** $k, l = 1 : n$ **do**

 Apply the protocol in Lemma 2 (if JW or BK mapping is applied) or in Lemma 3 (if TT is applied) for computing the quantities in (19)

 Use the quantities to compute the correlation functions (8)

end

else:

for $k, l = 1 : n$ **do**

 Apply the tomography in Lemma 4 for computing the quantities in (19)

 Use the quantities to compute the correlation functions (8)

end

where $c_i(t) := e^{iHt}c_i e^{-iHt}$ and ρ is the ground state of a quantum system. For a fixed time point t , we present a protocol that estimates the RGF's $\{G_{ab}^R(t)\}_{a,b=1}^n$ to additive error ϵ . Similar to Protocol 1, we consider the two regimes: $n \leq \frac{1}{\epsilon^2}$ and $n \geq \frac{1}{\epsilon^2}$.

We first consider the case where $n \leq \frac{1}{\epsilon^2}$. Unlike estimating the commutator correlation functions (15), in the anti-commutator case, no sample-efficient scheme may exist. Especially when JW or BK mapping is applied, we suggest to carry out the brute force measurement strategy, that is, measuring an observable at a time. The underlying reason is that, while the commutator case involves measuring 1-body fermionic observables composed of two Majorana operators, the anti-commutator case requires measuring individual Majorana operators. Moreover, the $2n$ Majorana operators mutually anticommute, and we cannot use simultaneous measurement strategies for mutually commuting Pauli observables. As a result, it may be hard to obtain any gain in sample complexity from existing shadow tomography strategies. On the other hand, we can reduce the number of circuits by considering the choice of fermion-to-qubit mapping together with proper shadow tomography techniques. For example, if the TT mapping is applied, using the approach in Lemma 3 as the same in Protocol 1 leads to a significant reduction of the number of measurement circuits from $\mathcal{O}(n^2)$ circuits for the brute force measurements to a single circuit with the random Pauli measurements.

1. Chained measurement strategy

Now we consider the other interesting case where $n \geq \frac{1}{\epsilon^2}$. In this case, we use the same protocol in Protocol 1 when the BK and TT mappings are considered, which is based on the protocol in [41]. However, when the JW mapping is applied, we can design a more efficient approach in terms of the number of circuits and circuit depth, without using a graph-theory algorithm like [41, Lemma 12]. In essence, our approach is divided into three steps as follows,

1. Estimate the magnitudes of Majorana operators under the JW mapping using the Bell sampling [32]
2. Throw away negligible observables and consider the remaining observables
3. Use a chained measurement strategy to determine the signs of the remaining observables.

The first two steps are typical in shadow tomography techniques based on Bell sampling [32, 41]. In the first step, we consider the following Pauli observables,

$$\{X_1, Z_1 X_2, \dots, Z_1 \cdots Z_{n-1} X_n, Y_1, Z_1 Y_2, \dots, Z_1 \cdots Z_{n-1} Y_n\}, \quad (21)$$

two of which reproduces the Majorana operators under the JW mapping. Notice that these observables mutually anticommute. Denoting this set of observables by $\{P_i\}_{i=1}^{2n}$, we apply the known Bell sampling procedure [32, 41] to the set $\{P_i \otimes P_i\}_{i=1}^{2n}$, and in the second step, neglect the observables that are estimated to have magnitudes less than $\frac{3\epsilon}{4}$.

For the last step, we introduce a variant of the Bell sampling strategy with more technical detail in Appendix C. Here we provide a brief intuition behind the strategy. In the known Bell sampling strategy, we construct the mutually-commuting observables $\{P_i \otimes P_i\}_{i=1}^{2n}$. Instead of this, we consider the following construction of observables,

$$P_1 \otimes P_2, P_2 \otimes P_3, \dots, P_{2n-1} \otimes P_{2n}. \quad (22)$$

Notice that these observables mutually commute, since P_j 's mutually anticommute. Thus, we can estimate these observables simultaneously. With this in mind, if we estimate the sign of P_1 , then we can infer that of P_2 from the estimation of $P_1 \otimes P_2$, that of P_3 from $P_2 \otimes P_3$, and so on. We call this a chained measurement strategy. In Appendix C, we discuss more detail for how to perform this chained measurement strategy. We here present a result for the proposed strategy as follows.

Lemma 5. *Assume that $n \geq \frac{1}{\epsilon^2}$ and the JW mapping is applied. Then, there exists a shadow tomography protocol that uses single-copy and two-copy measurements, and estimates the signs of the operators with $\mathcal{O}(\frac{\log n}{\epsilon^4})$ sample complexity, and $\mathcal{O}(1)$ circuits of $\mathcal{O}(1)$ depth.*

The proof of this lemma is shown in Appendix C. To put together, we obtain the following theorem that states the overall complexity of a protocol for estimating the RGF (20).

Theorem 2. *There exists a shadow tomography protocol that uses at most two-copy measurements, and estimates the RGF (20) to additive error ϵ with sample complexity $\mathcal{O}(\frac{n^2 \log n}{\epsilon^2})$ when $n \leq \frac{1}{\epsilon^2}$, and $\mathcal{O}(\frac{n \log n}{\epsilon^4})$ when $n \geq \frac{1}{\epsilon^2}$.*

Proof. We first choose either of the representations (11) or (12) based on the majority rule in Lemma 1. Without loss of generality, we assume the plus representation (11). In the representation, we let $A = c_i$ and $B = c_j^\dagger$, and consider the following three terms

$$\begin{aligned} \text{tr}(\rho_1 A), \quad \rho_1 &= \rho_+ \\ \text{tr}(\rho_2 A), \quad \rho_2 &= e^{-iHt} \rho e^{iHt} \\ \text{tr}(\rho_3 A), \quad \rho_3 &= e^{-iHt} B \rho B e^{iHt}. \end{aligned} \quad (23)$$

By fixing B , we perform the brute force strategy of measuring an observable at a time when $n \leq \frac{1}{\epsilon^2}$ and JW or BK is used, three times respectively with the three quantum states ρ_i ($i = 1, 2, 3$). If TT is used, we use the dynamic circuit strategy in Lemma 3. Similarly, in the regime where $n \geq \frac{1}{\epsilon^2}$, when JW is used, we apply the protocol in Lemma 5. If BK or TT is used, we use the same protocol as in Protocol 1. Therefore, when $n \leq \frac{1}{\epsilon^2}$, $\mathcal{O}(\frac{n \log n}{\epsilon^2})$ samples suffice, and $\mathcal{O}(\frac{\log n}{\epsilon^4})$ in the other scenario. Since there are $\mathcal{O}(n)$ choices for B , the total sample complexity for estimating the RGFs (20) scales as $\mathcal{O}(\frac{n^2 \log n}{\epsilon^2})$ when $n \leq \frac{1}{\epsilon^2}$ and $\mathcal{O}(\frac{n \log n}{\epsilon^4})$ when $n \geq \frac{1}{\epsilon^2}$, respectively. \square

Protocol 2: Fermionic-adapted shadow tomography 2 (FAST 2)

Data: Given initial state ρ , precision $\epsilon > 0$

Result: approximate the RGF (20) for any a, b

If $n \leq \frac{1}{\epsilon^2}$:

for $b = 1 : n$ **do**

Perform the brute force measurement strategy (if JW or BK mapping is applied) or the tomography method in Lemma 3 (if TT is applied) for computing the quantities in (23) and choosing either of the representations (11) or (12).
 Use the quantities to compute the RGFs with the resulting representation.

end

else:

for $b = 1 : n$ **do**

Apply the tomography in Lemma 5 (if TT mapping is applied) or the method in Lemma 4 (if JW or BK is used) for computing the quantities in (23) and choosing either of the representations (11) or (12).
 Use the quantities to compute the RGFs with the resulting representation.

end

We remark that unlike the commutator case in Protocol 1, there is an additional step of selecting either of the representations (11) or (12) in Protocol 2. To highlight, this additional step is simultaneously performed with the computation of the quantities in (23) without any further experiments, by doing post-processing on the measurement results. Specifically, the measure results involve the outcomes in the ancilla qubit, from which we count the number of $|0\rangle$ and $|1\rangle$ states and know whether ρ_+ in (11) appears more than ρ_- in (12) or vice versa, due to Lemma 1. By the majority rule, we therefore select either of the representations (11) or (12) without further experiments.

III. DISCUSSION

In this work, we present a framework for estimating the dynamical correlation functions using shadow tomography techniques. We introduce Fermionic-Adapted Shadow Tomography (FAST) protocols (Protocol 1 and Protocol 2), for efficiently estimating the commutator and anti-commutator correlation functions, respectively. The connection is established by reformulating these functions in a form amenable to direct measurement, thereby enabling their estimation via shadow tomography techniques. We expect the proposed protocols to be broadly applicable to practical problems in quantum simulation of many-body systems.

A. Comparison to the brute force measurement strategy and existing methods

A brute force strategy is to measure each observable respectively, based on the reformulated expressions of the correlation functions in (8), (11), or (12). However, this approach can be less efficient than our proposed protocols in general. For example, in the commutator case, the brute force approach incurs $\mathcal{O}(\frac{n^4 \log n}{\epsilon^2})$ sample complexity as in Table III, while Protocol 1 reduce the sample complexity by an order of one or two in terms of n , as shown in Table I. Furthermore, the number of measurement circuits is reduced by at least order of one in all cases. In the anti-commutator case, except when the Jordan-Wigner or Bravyi-Kitaev mapping is used, our protocols

reduce the sample complexity and the number of measurement circuits by an order of one in terms of n when $n \geq \frac{1}{\epsilon^2}$, as shown in Table I, Table II, and Table III. When $n \leq \frac{1}{\epsilon^2}$, while the sample complexity is comparable to the brute force approach, Protocol 2 can reduce the number of circuits by an order of one (TT, $n \leq \frac{1}{\epsilon^2}$), as shown in Table II.

In the recent works [35, 41], both approaches share a common strategy: they bypass Hamiltonian simulation by reformulating the correlation function, enabling the use of shadow tomography techniques. Although these approaches avoid the need for Hamiltonian simulation, they generally incur exponential sample complexity. Specifically, [41, Appendix B] explores shadow tomography protocols for the Green's functions by expressing them as Taylor series. However, their approach is restricted to specific classes of Hamiltonians, and is effective primarily for computing correlation functions near zero time, due to the super-exponential sample complexity with respect to the degree of Taylor-series approximation. On the other hand, the method in [35] is based on the continued fraction representations of correlation functions, which enables the estimation of Green's functions without Hamiltonian simulation. Nonetheless, the sample complexity of this approach increases exponentially with the level of continued fraction form. As a result, its applicability may be restricted to cases where a logarithmic level of continued fraction forms suffices. By contrast, our approach is more generally applicable and achieves polynomial sample complexity at the cost of requiring Hamiltonian simulation.

Correlation functions	Commutator		Anti-commutator	
Regime	$n \leq \frac{1}{\epsilon^2}$	$n \geq \frac{1}{\epsilon^2}$	$n \leq \frac{1}{\epsilon^2}$	$n \geq \frac{1}{\epsilon^2}$
Sample complexity	$\mathcal{O}(\frac{n^3 \log n}{\epsilon^2})$	$\mathcal{O}(\frac{n^2 \log n}{\epsilon^4})$	$\mathcal{O}(\frac{n^2 \log n}{\epsilon^2})$	$\mathcal{O}(\frac{n \log n}{\epsilon^4})$
Qubit count	n	$2n$	$n + 1$	$2n + 2$

TABLE I: Summary of Protocol 1 and Protocol 2 for estimating the correlation functions (15) and (20) in terms of sample complexity and the number of qubits required at most. If the number of qubits is n or $n + 1$, the protocols require only single-copy measurements, otherwise they involve two-copy measurements.

B. Future questions

The first question is whether the proposed protocols are nearly optimal, matching lower bounds for the sample complexity. Such a question for the case of simple measurements is addressed in [41], and it is wondered whether a similar analysis could be derived for the case of dynamical correlation functions. Secondly, could we extend the chained measurement strategy in Appendix C to the cases of the Bravyi-Kitaev and ternary tree mappings in order to reduce the number of circuits and execute them in a constant depth? Compared to the Jordan-Wigner mapping, these mappings exhibit the logarithmic scaling of the operator locality, and in several cases, lead to more efficient simulations on real quantum device [48, 56]. Developing better measurement protocols tailored to these two mappings is also an interesting future question.

Correlation functions	Commutator			Anti-commutator			
Regime	$n \leq \frac{1}{\epsilon^2}$	$n \leq \frac{1}{\epsilon^2}$	$n \geq \frac{1}{\epsilon^2}$	$n \leq \frac{1}{\epsilon^2}$	$n \leq \frac{1}{\epsilon^2}$	$n \geq \frac{1}{\epsilon^2}$	$n \geq \frac{1}{\epsilon^2}$
Mapping	JW,BK	TT	JW,BK,TT	JW,BK	TT	BK,TT	JW
Measurement	MMC	DC	B + MMC	NM	DC	B + NM	B + NM
Time complexity	$\mathcal{O}(n^6)$	$\mathcal{O}(1)$	$\mathcal{O}(\frac{n^5}{\epsilon^2})$	$\mathcal{O}(1)$	$\mathcal{O}(1)$	$\mathcal{O}(1)$	$\mathcal{O}(1)$
Circuit depth	$\mathcal{O}(n)$	$\mathcal{O}(1)$	$\mathcal{O}(n)$	$\mathcal{O}(1)$	$\mathcal{O}(1)$	$\mathcal{O}(n)$	$\mathcal{O}(1)$
Circuit count	$\mathcal{O}(n^3)$	$\mathcal{O}(n^2)$	$\mathcal{O}(\frac{n^2}{\epsilon^2})$	$\mathcal{O}(n^2)$	$\mathcal{O}(n)$	$\mathcal{O}(\frac{n}{\epsilon^2})$	$\mathcal{O}(n)$
Circuit	Fig. 1a	Fig. 1b	Fig. 1a, Fig. 1e	Fig. 1c	Fig. 1d	Fig. 1c, Fig. 1f	Fig. 1c, Fig. 1f

TABLE II: Summary of Protocol 1 and Protocol 2 for estimating the correlation functions (15) and (20) in terms of the fermion-to-qubit mapping, the types of measurements, the classical time complexity for constructing Clifford measurement circuits, the circuit depth required for the corresponding measurements, the number of circuits required for execution (circuit count), and the specific circuit implementations used for execution. The measurement types are abbreviated as follows: Clifford measurements for mutually commuting observables (MMC), random Pauli measurements combined with dynamic circuits (DC), Bell sampling (B), and brute force measurements in the computational basis (NM). As discussed in [41], techniques in the stabilizer formalism [1] can be used to construct a Clifford circuit for MMC within $\mathcal{O}(n^3)$ time. Therefore, in the cases where MMC is considered, the time complexity is estimated as $\mathcal{O}(n^3) \times$ Circuit count, since MMC is performed independently for each circuit in the protocols.

Correlation functions	Commutator	Anti-commutator
Sample complexity	$\mathcal{O}(\frac{n^4 \log n}{\epsilon^2})$	$\mathcal{O}(\frac{n^2 \log n}{\epsilon^2})$
Qubit count	n	$n + 1$
Time complexity	$\mathcal{O}(1)$	$\mathcal{O}(1)$
Circuit depth	$\mathcal{O}(1)$	$\mathcal{O}(1)$
Circuit count	$\mathcal{O}(n^4)$	$\mathcal{O}(n^2)$
Circuit	Fig. 1a	Fig. 1c

TABLE III: Summary of the brute force measurement strategies for computing the correlation functions (15) and (20). These approaches require only single-copy measurements.

IV. ACKNOWLEDGEMENT

We thank Dr. Eunwoo Lee, Prof. Hyukjoon Kwon, Dr. Gyungmin Cho for fruitful discussions during the early stages of this project.

Appendix A: The triply efficient shadow tomography for learning 1-body observables

In this section, we review on a specialized application of the shadow tomography protocol by King *et al* [41], in order to derive the result in Lemma 4.

Lemma 6. [41, Lemma 1] *The size of the largest clique in G_ϵ is at most $\frac{4}{\epsilon^2}$ with high probability.*

Lemma 7. [41, Lemma 12] Let G' be a subgraph of the commutation graph of $G(\mathcal{F}_1^{(n)})$ of 1-body observables, and ω is the size of the largest clique in G' . Then, there is a classical algorithm that outputs a coloring of G' with $\mathcal{O}(n^2\omega)$ runtime using at most $\omega + 1$ colors.

Using these lemmas, we prove Lemma 4, which follows from the original work [41].

Proof. Let G_ϵ be the subgraph of the commutation graph for the 1-body observables after thresholding observables of magnitudes less than ϵ .

By Lemma 6 and Lemma 7, coloring G_ϵ requires $\frac{4}{\epsilon^2} + 1$ colors, and for each color, there are at most $\mathcal{O}(n^2)$ observables, since the number of 1-body observables is $\mathcal{O}(n^2)$. This means that measuring the observables for each color requires $\mathcal{O}(\frac{\log \frac{n}{\epsilon}}{\epsilon^2})$ sample complexity using Clifford measurements [1]. Since there are $\mathcal{O}(\frac{1}{\epsilon^2})$ colors, the total sample complexity is $\mathcal{O}(\frac{\log \frac{n}{\epsilon}}{\epsilon^4})$. Since the number of 1-body observables scales as $\mathcal{O}(n^2)$, by setting the new failure probability as $\delta \leftarrow \frac{\delta}{n^2}$, we can learn the observables in G_ϵ with probability at least $1 - \delta$ using $\mathcal{O}(\frac{\log n}{\epsilon^4})$ samples, and $\mathcal{O}(\frac{1}{\epsilon^2})$ circuits corresponding to the colors. Therefore, measuring all observables in G_ϵ with single-copy measurements can be done with $\mathcal{O}(\frac{\log n}{\epsilon^4})$ sample complexity and $\mathcal{O}(\frac{1}{\epsilon^2})$ Clifford measurement circuits. \square

Appendix B: Measurement-based state preparation

Within the circuit Fig. 1c, the state is evolved as follows,

$$\begin{aligned}
& |0\rangle\langle 0| \otimes \rho \\
& \rightarrow |+\rangle\langle +| \otimes \rho \\
& \rightarrow |0\rangle\langle 0| \otimes \rho + |1\rangle\langle 0| \otimes B\rho + |0\rangle\langle 1| \otimes \rho B + |1\rangle\langle 1| \otimes B\rho B \\
& \rightarrow |0\rangle\langle 0| \otimes e^{iHt}\rho e^{-iHt} + |1\rangle\langle 0| \otimes e^{iHt}B\rho e^{-iHt} + |0\rangle\langle 1| \otimes e^{iHt}\rho B e^{-iHt} + |1\rangle\langle 1| \otimes e^{iHt}B\rho B e^{-iHt} \\
& \rightarrow |+\rangle\langle +| \otimes e^{iHt}\rho e^{-iHt} + |-\rangle\langle +| \otimes e^{iHt}B\rho e^{-iHt} + |+\rangle\langle -| \otimes e^{iHt}\rho B e^{-iHt} + |-\rangle\langle -| \otimes e^{iHt}B\rho B e^{-iHt} \\
& \implies \rho_+ \text{ if 0 in the ancilla with probability } C_+^2, \rho_- \text{ if 1 in the ancilla with probability } C_-^2,
\end{aligned} \tag{B1}$$

where ρ_\pm and C_\pm are defined in (11) and (12). Similarly, we can obtain states ρ_\pm within the circuits Fig. 1d, and Fig. 1f.

Appendix C: Chained measurement strategy for the JW-mapped Majorana operators

In this section, we prove Lemma 5. To proceed, we first consider the following preliminary exercise.

For the independent events that $A = 1$ and $B = 1$, we let $\mathbb{P}(A = 1) \geq 1 - \delta_1$ and $\mathbb{P}(B = 1) \geq 1 - \delta_2$. Then, we have

$$\mathbb{P}(AB = 1) \geq \mathbb{P}(A = 1, B = 1) = \mathbb{P}(A = 1)\mathbb{P}(B = 1) \geq (1 - \delta_1)(1 - \delta_2). \tag{C1}$$

This implies that if random variables, \hat{a} and \hat{b} , satisfy that $\text{sign}(\hat{a}) = \text{sign}(a)$ and $\text{sign}(\hat{b}) = \text{sign}(b)$ with high probability for the corresponding true values, a and b , then $\text{sign}(\hat{a}\hat{b}) = \text{sign}(ab)$ with h.p. This can be understood by setting $A = \text{sign}(\hat{a})\text{sign}(a)$ and $B = \text{sign}(\hat{b})\text{sign}(b)$.

The RGF calculations in (20) consider the annihilation and creation observables, which are represented by the Majorana operators under the JW mapping

$$S_X := \{X_1, Z_1 X_2, \dots, Z_1 \cdots Z_{n-1} X_n\}, \quad S_Y := \{Y_1, Z_1 Y_2, \dots, Z_1 \cdots Z_{n-1} Y_n\}. \quad (\text{C2})$$

For convenience, we denote $\{P_i\}_{i=1}^n$ and $\{Q_i\}_{i=1}^n$ to be the sets S_X and S_Y . The indices are arranged consistently with the elements of the sets. For example, $P_1 = X_1$, $P_3 = Z_1 Z_2 X_3$, $Q_n = Z_1 \cdots Z_{n-1} Y_n$, and so forth. Notice that the observables in both sets mutually anticommute. In this case, the use of the coloring strategy [41] does not give any efficiency for the problem here, since any subset of the Majorana observables consists of mutually anticommuting Paulis.

Here we introduce a novel shadow tomography protocol based on Bell sampling. Our protocol is tailored to the set of Majorana observables in (C2). Suppose that the Bell sampling for neglecting observables of small magnitudes is already performed [32, 41]. We let $\{P_{r_i}\}_{i=1}^I$ and $\{Q_{k_j}\}_{j=1}^J$ be the remaining observables as subsets of S_X and S_Y , respectively, where r_i 's and k_j 's are arranged in increasing order. We define the two sets of observables as follows,

$$B_X := \{P_{r_i} \otimes P_{r_{i+1}} : i \in [I-1]\}, \quad B_Y := \{Q_{k_j} \otimes Q_{k_{j+1}} : j \in [J-1]\}. \quad (\text{C3})$$

In the following, we show that a property of the two sets (C3),

Lemma 8. *The Pauli strings in B_X mutually commute with the common eigenstates as follows,*

$$\{|Bell\rangle_{r_1, n+r_2} |Bell\rangle_{r_2, n+r_3} \cdots |Bell\rangle_{r_{I-1}, n+r_I} |b\rangle : b \text{ is the computational basis on the remaining qubits}\}, \quad (\text{C4})$$

where $|Bell\rangle_{a,b}$ denotes the four possible Bell states acting on qubit a and qubit b . Similarly, the Pauli strings in B_Y have eigenstates as

$$\{|Bell\rangle_{k_1, n+k_2} |Bell\rangle_{k_2, n+k_3} \cdots |Bell\rangle_{k_{J-1}, n+k_J} |b\rangle : b \text{ is the computational basis on the remaining qubits}\}. \quad (\text{C5})$$

Proof. We prove the statement by induction on the cardinality of set B_X . For $I = 3$, it is trivial. Suppose the statement holds up to $I \leq \mathfrak{J}$. We consider the case $I = \mathfrak{J} + 1$ and denote the corresponding set by B . Using the hypothesis for the subset of B , which consists of the first \mathfrak{J} elements of B , we let $v = |Bell\rangle_{r_1, n+r_2} |Bell\rangle_{r_2, n+r_3} \cdots |Bell\rangle_{r_{\mathfrak{J}-2}, n+r_{\mathfrak{J}-1}} |b\rangle$, a Bell basis element. \square

Now we prove Lemma 5 using Lemma 8.

Proof. For a given state ρ , our goal is to estimate the Majorana observables in (C2), that is, $\text{tr}(\rho O)$ for each $O \in S_X \cup S_Y$. We perform single-copy measurements and two-copy measurements as follows,

1. Estimate the magnitudes of expectations of observables in (C2) to precision ϵ
(Two-copy measurements with $\mathcal{O}(\frac{\log n}{\epsilon^4})$ sample complexity)
2. Throw away observables having small magnitudes ($\leq \frac{3\epsilon}{4}$).
($\mathcal{O}(n)$ classical time)
3. Let us consider the remaining observables, denoted as $\{P_{r_i}\}_{i=1}^I$ and $\{Q_{k_j}\}_{j=1}^J$ in (C3).

4. Measure the first observables, P_{r_1}, Q_{k_1} , to precision ϵ^2 , $\text{tr}(\rho P_{r_1})$ and $\text{tr}(\rho Q_{k_1})$.
(Single-copy measurements with $\mathcal{O}(\frac{1}{\epsilon^2})$ sample complexity)
5. Measure the observables in (C3) to precision ϵ^2 using the measurement basis in Lemma 8.
(Two-copy measurements with $\mathcal{O}(\frac{\log \min\{n, \max\{I, J\}\}}{\epsilon^4})$ sample complexity, where $I, J \leq n$)

In total, our protocol incurs $\mathcal{O}(\frac{\log n}{\epsilon^4})$ sample complexity and $\mathcal{O}(n)$ classical time cost, and $\mathcal{O}(1)$ circuits.

From the data analysis point of view, we perform three independent experiments (i.e. step 1, step 4, step 5 in the above protocol). The first experiment gives us the estimates of magnitudes, $\{p_{r_i}^{(1)}\}, \{q_{k_j}^{(1)}\}$ with probability at least $1 - \delta_1$

$$|\text{tr}(\rho P_{r_i})|, |\text{tr}(\rho Q_{k_j})| \geq \frac{\epsilon}{2}, \left| p_{r_i}^{(1)} - |\text{tr}(\rho P_{r_i})| \right| \leq \frac{\epsilon}{4}, \left| q_{k_j}^{(1)} - |\text{tr}(\rho Q_{k_j})| \right| \leq \frac{\epsilon}{4}, \quad (\text{C6})$$

the second experiment produces the estimates of the first observables, $p_{r_1}^{(2)}, q_{k_1}^{(2)}$, with probability at least $1 - \delta_2$

$$\left| p_{r_1}^{(2)} - \text{tr}(\rho P_{r_1}) \right| \leq \frac{\epsilon}{4}, \left| q_{k_1}^{(2)} - \text{tr}(\rho Q_{k_1}) \right| \leq \frac{\epsilon}{4}, \quad (\text{C7})$$

and the last gives the estimates of the chained trace multiplications, $\{p_{r_i}^{(3)}\}, \{q_{k_j}^{(3)}\}$, with probability at least $1 - \delta_3$

$$\left| p_{r_i, r_{i+1}}^{(3)} - \text{tr}(\rho P_{r_i}) \text{tr}(\rho P_{r_{i+1}}) \right| \leq \frac{\epsilon^2}{8}, \left| q_{k_j, k_{j+1}}^{(3)} - \text{tr}(\rho Q_{k_j}) \text{tr}(\rho Q_{k_{j+1}}) \right| \leq \frac{\epsilon^2}{8}. \quad (\text{C8})$$

Since the events in (C6), (C7), (C8) happens independently. the above inequalities hold simultaneously with probability at least $(1 - \delta_1)(1 - \delta_2)(1 - \delta_3)$.

We claim that from the inequalities, we can estimate the Majorana observables in (C2). From (C6), we estimate the magnitudes of expectation values of observables, and consider only the observables of magnitudes no less than $\frac{3\epsilon}{4}$. From (C7), we estimate the signs of the first expectation values. With (C6) and (C8), we know that $\{p_{r_i}^{(3)}\}, \{q_{k_j}^{(3)}\}$ have the same sign as the corresponding true values. For example, (C6) implies that

$$|\text{tr}(\rho P_{r_i}) \text{tr}(\rho P_{r_{i+1}})| \geq \frac{\epsilon^2}{4}, \quad (\text{C9})$$

and from (C8), we see that

$$\left| p_{r_i, r_{i+1}}^{(3)} - \text{tr}(\rho P_{r_i}) \text{tr}(\rho P_{r_{i+1}}) \right| \leq \frac{\epsilon^2}{8}. \quad (\text{C10})$$

Therefore, the signs of the estimate $p_{r_i, r_{i+1}}^{(3)}$ and the corresponding true value $\text{tr}(\rho P_{r_i}) \text{tr}(\rho P_{r_{i+1}})$ are the same. It is the same for the other estimates in (C8). Together with (C7) and (C1), we estimate the signs of the estimates in (C6) by tracking the sign of $p_{r_1}^{(2)} p_{r_1, r_2}^{(3)}$, that of $p_{r_1}^{(2)} p_{r_1, r_2}^{(3)} p_{r_2, r_3}^{(3)}$, and so forth. Therefore, we prove the claim and completes the proof of Lemma 5. \square

-
- [1] Scott Aaronson and Daniel Gottesman. Improved simulation of stabilizer circuits. *Physical Review A—Atomic, Molecular, and Optical Physics*, 70(5):052328, 2004.
 - [2] Christian Kraglund Andersen, Ants Remm, Stefania Lazar, Sebastian Krinner, Johannes Heinsoo, Jean-Claude Besse, Mihai Gabureac, Andreas Wallraff, and Christopher Eichler. Entanglement stabilization using ancilla-based parity detection and real-time feedback in superconducting circuits. *npj Quantum Information*, 5(1):69, 2019.
 - [3] Alán Aspuru-Guzik, Anthony D Dutoi, Peter J Love, and Martin Head-Gordon. Simulated quantum computation of molecular energies. *Science*, 309(5741):1704–1707, 2005.
 - [4] Bela Bauer, Sergey Bravyi, Mario Motta, and Garnet Kin-Lic Chan. Quantum algorithms for quantum chemistry and quantum materials science. *Chemical reviews*, 120(22):12685–12717, 2020.
 - [5] Bela Bauer, Dave Wecker, Andrew J Millis, Matthew B Hastings, and Matthias Troyer. Hybrid quantum-classical approach to correlated materials. *Physical Review X*, 6(3):031045, 2016.
 - [6] Elisa Bäumer, Vinay Tripathi, Alireza Seif, Daniel Lidar, and Derek S Wang. Quantum fourier transform using dynamic circuits. *Physical Review Letters*, 133(15):150602, 2024.
 - [7] Elisa Bäumer, Vinay Tripathi, Derek S Wang, Patrick Rall, Edward H Chen, Swarnadeep Majumder, Alireza Seif, and Zlatko K Minev. Efficient long-range entanglement using dynamic circuits. *PRX Quantum*, 5(3):030339, 2024.
 - [8] Gordon Baym and Leo P. Kadanoff. Conservation Laws and Correlation Functions. 124(2):287–299.
 - [9] Christian Bertoni, Jonas Haferkamp, Marcel Hinsche, Marios Ioannou, Jens Eisert, and Hakop Pashayan. Shallow shadows: Expectation estimation using low-depth random clifford circuits. *Physical Review Letters*, 133(2):020602, 2024.
 - [10] Xavier Bonet-Monroig, Ryan Babbush, and Thomas E O’Brien. Nearly optimal measurement scheduling for partial tomography of quantum states. *Physical Review X*, 10(3):031064, 2020.
 - [11] Sergey B Bravyi and Alexei Yu Kitaev. Fermionic quantum computation. *Annals of Physics*, 298(1):210–226, 2002.
 - [12] Marco Cerezo, Akira Sone, Tyler Volkoff, Lukasz Cincio, and Patrick J Coles. Cost function dependent barren plateaus in shallow parametrized quantum circuits. *Nature communications*, 12(1):1791, 2021.
 - [13] Hongxiang Chen, Max Nusspickel, Jules Tilly, and George H Booth. Variational quantum eigensolver for dynamic correlation functions. *Physical Review A*, 104(3):032405, 2021.
 - [14] Alessandro Chiesa, Francesco Tacchino, Michele Grossi, Paolo Santini, Ivano Tavernelli, Dario Gerace, and Stefano Carretta. Quantum hardware simulating four-dimensional inelastic neutron scattering. *Nature Physics*, 15(5):455–459, 2019.
 - [15] Gyungmin Cho and Dohun Kim. Entanglement-enhanced randomized measurement in noisy quantum devices. *arXiv preprint arXiv:2504.15698*, 2025.
 - [16] Talal Ahmed Chowdhury, Kwangmin Yu, and Raza Sabbir Sufian. First measurement of entanglement dynamics in the syk model using quantum computers. *arXiv preprint arXiv:2503.18580*, 2025.
 - [17] Laura Clinton, Johannes Bausch, and Toby Cubitt. Hamiltonian simulation algorithms for near-term quantum hardware. *Nature communications*, 12(1):4989, 2021.
 - [18] Mirko Consiglio, Jacopo Settimo, Andrea Giordano, Carlo Mastroianni, Francesco Plastina, Salvatore Lorenzo, Sabrina Maniscalco, John Goold, and Tony JG Apollaro. Variational gibbs state preparation on noisy intermediate-scale quantum devices. *Physical Review A*, 110(1):012445, 2024.
 - [19] Antonio D Córcoles, Maika Takita, Ken Inoue, Scott Lekuch, Zlatko K Minev, Jerry M Chow, and Jay M Gambetta. Exploiting dynamic quantum circuits in a quantum algorithm with superconducting qubits. *Physical Review Letters*, 127(10):100501, 2021.
 - [20] Pierre-Luc Dallaire-Demers and Frank K Wilhelm. Quantum gates and architecture for the quantum simulation of the fermi-hubbard model. *Physical Review A*, 94(6):062304, 2016.
 - [21] Zhiyan Ding, Xiantao Li, and Lin Lin. Simulating open quantum systems using hamiltonian simulations. *PRX quantum*, 5(2):020332, 2024.
 - [22] Suguru Endo, Iori Kurata, and Yuya O Nakagawa. Calculation of the green’s function on near-term quantum computers. *Physical Review Research*, 2(3):033281, 2020.

- [23] César Feniou, Olivier Adjoua, Baptiste Claudon, Julien Zylberman, Emmanuel Giner, and Jean-Philip Piquemal. Sparse quantum state preparation for strongly correlated systems. *The Journal of Physical Chemistry Letters*, 15(11):3197–3205, 2024.
- [24] Ryan R Ferguson, Luca Dellantonio, A Al Balushi, Karl Jansen, Wolfgang Dür, and Christine A Muschik. Measurement-based variational quantum eigensolver. *Physical review letters*, 126(22):220501, 2021.
- [25] Pranav Gokhale, Olivia Angiuli, Yongshan Ding, Kaiwen Gui, Teague Tomesh, Martin Suchara, Margaret Martonosi, and Frederic T Chong. Optimization of simultaneous measurement for variational quantum eigensolver applications. In *2020 IEEE international conference on Quantum Computing and Engineering (QCE)*, pages 379–390. IEEE, 2020.
- [26] Niladri Gomes, David B Williams-Young, and Wibe A de Jong. Computing the many-body green’s function with adaptive variational quantum dynamics. *Journal of Chemical Theory and Computation*, 19(11):3313–3323, 2023.
- [27] Ikko Hamamura and Takashi Imamichi. Efficient evaluation of quantum observables using entangled measurements. *npj Quantum Information*, 6(1):56, 2020.
- [28] Mancheon Han, Hyowon Park, and Sangkook Choi. Quantum zeno monte carlo for computing observables. *npj Quantum Inf.*, 11(arXiv: 2403.02763):46, 2025.
- [29] Vojtěch Havlíček, Matthias Troyer, and James D Whitfield. Operator locality in the quantum simulation of fermionic models. *Physical Review A*, 95(3):032332, 2017.
- [30] Hong-Ye Hu, Andi Gu, Swarnadeep Majumder, Hang Ren, Yipei Zhang, Derek S Wang, Yi-Zhuang You, Zlatko Mineev, Susanne F Yelin, and Alireza Seif. Demonstration of robust and efficient quantum property learning with shallow shadows. *Nature Communications*, 16(1):2943, 2025.
- [31] Hsin-Yuan Huang, Richard Kueng, and John Preskill. Predicting many properties of a quantum system from very few measurements. *Nature Physics*, 16(10):1050–1057, 2020.
- [32] Hsin-Yuan Huang, Richard Kueng, and John Preskill. Information-theoretic bounds on quantum advantage in machine learning. *Physical Review Letters*, 126(19):190505, 2021.
- [33] William J Huggins, Kianna Wan, Jarrod McClean, Thomas E O’Brien, Nathan Wiebe, and Ryan Babbush. Nearly optimal quantum algorithm for estimating multiple expectation values. *Physical Review Letters*, 129(24):240501, 2022.
- [34] Tatsuhiko N Ikeda, Hideki Kono, and Keisuke Fujii. Measuring trotter error and its application to precision-guaranteed hamiltonian simulations. *Physical Review Research*, 6(3):033285, 2024.
- [35] Reinis Irmejs and Raul A Santos. Approximating dynamical correlation functions with constant depth quantum circuits. *Quantum*, 9:1639, 2025.
- [36] Artur F Izmaylov, Tzu-Ching Yen, Robert A Lang, and Vladyslav Verteletskyi. Unitary partitioning approach to the measurement problem in the variational quantum eigensolver method. *Journal of chemical theory and computation*, 16(1):190–195, 2019.
- [37] Zhang Jiang, Amir Kalev, Wojciech Mruczkiewicz, and Hartmut Neven. Optimal fermion-to-qubit mapping via ternary trees with applications to reduced quantum states learning. *Quantum*, 4:276, 2020.
- [38] Shi Jin and Xiantao Li. A partially random trotter algorithm for quantum hamiltonian simulations. *Communications on Applied Mathematics and Computation*, 7(2):442–469, 2025.
- [39] Shota Kanasugi, Shoichiro Tsutsui, Yuya O Nakagawa, Kazunori Maruyama, Hirotaka Oshima, and Shintaro Sato. Computation of green’s function by local variational quantum compilation. *Physical Review Research*, 5(3):033070, 2023.
- [40] Shu Kanno, Ikko Hamamura, Rudy Raymond, Qi Gao, and Naoki Yamamoto. Efficient implementation of randomized quantum algorithms with dynamic circuits. *arXiv preprint arXiv:2503.17833*, 2025.
- [41] Robbie King, David Gosset, Robin Kothari, and Ryan Babbush. Triply efficient shadow tomography. In *Proceedings of the 2025 Annual ACM-SIAM Symposium on Discrete Algorithms (SODA)*, pages 914–946. SIAM, 2025.
- [42] Efehan Kökcü, Heba A Labib, JK Freericks, and Alexander F Kemper. A linear response framework for quantum simulation of bosonic and fermionic correlation functions. *Nature Communications*, 15(1):3881, 2024.
- [43] Taichi Kosugi and Yu-ichiro Matsushita. Linear-response functions of molecules on a quantum com-

- puter: Charge and spin responses and optical absorption. *Physical Review Research*, 2(3):033043, 2020.
- [44] James B Larsen, Matthew D Grace, Andrew D Baczewski, and Alicia B Magann. Feedback-based quantum algorithms for ground state preparation. *Physical Review Research*, 6(3):033336, 2024.
 - [45] Seth Lloyd. Universal quantum simulators. *Science*, 273(5278):1073–1078, 1996.
 - [46] J. M. Luttinger and J. C. Ward. Ground-State Energy of a Many-Fermion System. II. 118(5):1417–1427.
 - [47] Gerald D Mahan. *Many-particle physics*. Springer Science & Business Media, 2013.
 - [48] Aaron Miller, Zoltán Zimborás, Stefan Knecht, Sabrina Maniscalco, and Guillermo García-Pérez. Bon-sai algorithm: Grow your own fermion-to-qubit mappings. *PRX quantum*, 4(3):030314, 2023.
 - [49] Martin Mootz, Thomas Iadecola, and Yong-Xin Yao. Adaptive variational quantum computing approaches for green’s functions and nonlinear susceptibilities. *Journal of Chemical Theory and Computation*, 20(19):8689–8710, 2024.
 - [50] Ramil Nigmatullin, Kevin Hemery, Khaldoon Ghanem, Steven Moses, Dan Gresh, Peter Siegfried, Michael Mills, Thomas Gatterman, Nathan Hewitt, Etienne Granet, et al. Experimental demonstration of break-even for the compact fermionic encoding. *arXiv preprint arXiv:2409.06789*, 2024.
 - [51] Samuele Piccinelli, Francesco Tacchino, Ivano Tavernelli, and Giuseppe Carleo. Efficient calculation of green’s functions on quantum computers via simultaneous circuit perturbation. *arXiv preprint arXiv:2505.05563*, 2025.
 - [52] M. Potthoff. Self-energy-functional approach to systems of correlated electrons. 32(4):429–436.
 - [53] David Poulin, Matthew B Hastings, Dave Wecker, Nathan Wiebe, Andrew C Doherty, and Matthias Troyer. The trotter step size required for accurate quantum simulation of quantum chemistry. *arXiv preprint arXiv:1406.4920*, 2014.
 - [54] Ho Lun Tang, VO Shkolnikov, George S Barron, Harper R Grimsley, Nicholas J Mayhall, Edwin Barnes, and Sophia E Economou. qubit-adapt-vqe: An adaptive algorithm for constructing hardware-efficient ansätze on a quantum processor. *PRX Quantum*, 2(2):020310, 2021.
 - [55] Yu Tong, Dong An, Nathan Wiebe, and Lin Lin. Fast inversion, preconditioned quantum linear system solvers, fast green’s-function computation, and fast evaluation of matrix functions. *Physical Review A*, 104(3):032422, 2021.
 - [56] Andrew Tranter, Peter J Love, Florian Mintert, and Peter V Coveney. A comparison of the bravyi–kitaev and jordan–wigner transformations for the quantum simulation of quantum chemistry. *Journal of chemical theory and computation*, 14(11):5617–5630, 2018.
 - [57] Pengfei Wang, Hyukjoon Kwon, Chun-Yang Luan, Wentao Chen, Mu Qiao, Zinan Zhou, Kaizhao Wang, MS Kim, and Kihwan Kim. Snapshotting quantum dynamics at multiple time points. *Nature Communications*, 15(1):8900, 2024.
 - [58] Qing Xie, Kazuhiro Seki, and Seiji Yunoki. Variational counterdiabatic driving of the hubbard model for ground-state preparation. *Physical Review B*, 106(15):155153, 2022.
 - [59] Andrew Zhao, Nicholas C Rubin, and Akimasa Miyake. Fermionic partial tomography via classical shadows. *Physical Review Letters*, 127(11):110504, 2021.
 - [60] Andrew Zhao, Andrew Tranter, William M Kirby, Shu Fay Ung, Akimasa Miyake, and Peter J Love. Measurement reduction in variational quantum algorithms. *Physical Review A*, 101(6):062322, 2020.
 - [61] Linghua Zhu, Senwei Liang, Chao Yang, and Xiaosong Li. Optimizing shot assignment in variational quantum eigensolver measurement. *Journal of Chemical Theory and Computation*, 20(6):2390–2403, 2024.
 - [62] Sergiy Zhuk, Niall F Robertson, and Sergey Bravyi. Trotter error bounds and dynamic multi-product formulas for hamiltonian simulation. *Physical Review Research*, 6(3):033309, 2024.